Measurements of turbulence generated by oscillating grid

Cheng, Nian-Sheng; Law, Adrian Wing-Keung

2001

Cheng, N. S., & Law, A. W. K. (2001). Measurements of turbulence generated by oscillating grid. Journal of Hydraulic Engineering, 127(3), 201-208.

https://hdl.handle.net/10356/83698

https://doi.org/10.1061/(ASCE)0733-9429(2001)127:3(201)

MEASUREMENTS OF TURBULENCE GENERATED BY OSCILLATING GRID

By Nian-Sheng Cheng[1] and Adrian Wing-Keung Law[2]

ABSTRACT: Turbulence generated by a vertically oscillating grid in a water tank was investigated using the DPIV technique. The statistical turbulence characteristics computed based on the experimental data agree well with the two main findings reported in the literature, i.e., the turbulence decays following the power law and the integral length scale increases linearly with the distance from the grid. In addition, the flow structure near the grid was observed in details with the advantage of the planar measurements. It was found that the velocity fluctuations in the region near the grid vary depending on the grid geometry. The fluctuations immediately over the bar position are significantly different from those over the grid openings. Turbulence with the highest intensity occurs above the intersection of the square bars that constitute the grid. The results imply that shear flow clearly exists near the grid and homogeneity of the turbulence can only be achieved at a distance from the grid greater than about three mesh sizes. In addition, it was found that at least 400 vector maps should be taken to ensure the accuracy of the measured velocity fluctuations.

Keywords: DPIV, Flow measurement, grid turbulence, homogeneity, turbulence decay, Reynolds stress, and integral scale.

INTRODUCTION

Turbulence generated by an oscillating grid in a water tank has been used in various laboratory settings. Rouse (1939) appeared to be the first to employ this confined turbulent environment to study the characteristics of sediment suspension. Subsequent studies on particle-turbulence interaction include Ettema et al. (1984), Nielson (1993) and

---

[1] Research Fellow, School of Civil and Structural Engineering, Nanyang Technological University, Nanyang Avenue, Singapore 639798.

[2] Assoc. Professor, School of Civil and Structural Engineering, Nanyang Technological University, Nanyang Avenue, Singapore 639798.

Lyn (1995). Ettema et al.'s study concerned the dependence of the rate and the quantity of frazil ice growth on the turbulence intensity. Nielsen observed the effect of turbulence on the settling velocity of suspended particles, while Lyn (1995) utilised the grid turbulence to study the initiation of sediment transport. Grid turbulence is also often employed to address the interfacial mixing in stratified fluids that widely exists in the ocean, the atmosphere and lakes. Pioneer works in this area were conducted by Thompson and Turner (1975) and Hopfinger and Toly (1976), who explored the spatial decay of turbulence and entrainment across a salinity interface. Similar experiments have also been performed to study the free-surface affected turbulence and the gas transfer processes at the gas/water interface (Brumley and Jirka 1987; Jirka 1991). In addition, Brunk et al. (1996) considered that grid-generated turbulence, as a self-contained system, is particularly suitable for studies in environmental engineering because it provides an ideal environment for the investigations of physical and chemical processes of pollutants over long time spans, which would otherwise require an unacceptably long channel in a conventional flume-type system. The incorporation of different time scales is necessary for the transport of pollutants that undergoes various processes such as turbulent diffusion, coagulation and settling.

In comparison with turbulence in boundary layers and open channels, the turbulence generated by an oscillating grid is considered to be theoretically simpler, being characterised by zero-mean velocity and homogeneity. However, such grid-induced turbulence is also complex with obvious influences by the shape and size of the grid, and the stroke and frequency of oscillation. Fortunately, in most of the previous studies, for example, Thompson and Turner (1975), Hopfinger and Toly (1976), McDougal (1979), Nokes (1988), De Silva and Fernando (1992) and Lyn (1997), the grids used are rather similar (see Table 1). This allows a direct comparison of the results obtained in these studies. However, even with the extensive database available, a number of questions remain regarding the characteristics of this mechanically driven turbulence.

The early measurements of grid-induced turbulence were performed with a hot-film probe mounted on a spindle, which rotated on a plane parallel to the grid (Thompson and Turner 1975; Hopfinger and Toly 1976). These measurements directly yielded spatially averaged velocities. However, the rotating probe is intrusive and its effect on the turbulence measurements is not clear. Thompson and Turner (1975) demonstrated that for a grid made of square bars, the integral turbulence length scale increased linearly with the distance from the grid, z, while the r.m.s. horizontal velocity, u, decayed with distance from the grid to the power of -1.5. Their results also showed that the power had to be much less negative than -1.5 to describe the decay in the region close to the grid. Hopfinger and Toly (1976) confirmed the linear dependence of the turbulence length scale on the distance from the grid. However, they proposed that u should instead decay in the form

$$u = CfS^{1.5}M^{0.5}z_v^{-n} \tag{1}$$

where C = 0.25, n = 1, f = frequency, S = stroke, M = mesh size defined as the distance between the centres of two neighbouring openings, and z_v = distance from a virtual origin near the mid-position of the grid. Hopfinger and Toly thus concluded that the turbulent kinetic energy, k, decays approximately with z according to a power law, $k \propto z^{-2}$, and that the turbulent Reynolds number, defined as ul/v where l = integral length scale and v = kinematic viscosity of fluid, remains approximately constant during the decay. To maximise the agreement of the measurements with the proposed power law, both Thompson and Turner (1975) and Hopfinger and Toly (1976) adopted a virtual origin instead of the mid-position of the grid for measuring the distance. Thompson and Turner reported that the virtual origin should be generally below the grids, with 1cm and 2cm for the square-barred and round-barred grids, respectively. In comparison, Hopfinger and Toly defined the virtual origin as the height in the fluid where the integral length scale became zero, which was computed to be slightly below the mid-position. Generally, the power *n* in (1) is very sensitive to the position of the virtual origin. This may be one of the reasons that various forms of the power laws have been reported in the literature.

Besides the measurements with the hot-film probe as described above, grid turbulence has also been investigated using other techniques such as LDV (e.g. McDougal 1979; De Silva and Fernando 1992), ADV (Brunk et al. 1996), and PIV (Lyn 1997). McDougal (1979) found that the turbulence generated with 1 cm stroke was far from homogeneous in the horizontal plane. His results also showed that the upper limit of the oscillating frequency was approximately 7 Hz, above which a large circulating motion occurred and the u-value would no longer be linearly related to frequency. Brunk et al. (1996) used five horizontally oscillating grids to simulate the hydrodynamic and chemical processes associated with pollutant fate in aquatic environments. Despite the very different grid arrangement, their results on the turbulence kinetic energy are close to those obtained earlier by Hopfinger and Toly (1976). Lyn (1997) measured the oscillating-grid turbulence using the PIV technique and reported that the spatially averaged characteristics agreed with previous works, while the time-averaged results at a single section implied strong and persistent large-scale motion. However, the accuracy of his statistical results may be notably affected by the small number of images taken, which only ranged from 25 to 36. The effect of the sampling duration and frequency for the PIV measurements is addressed further in this paper.

Instead of directly measuring the variation of the velocity fluctuations with the distance from the grid, Nokes (1988) deduced the value of the decay power in (1) using the experiment data of entrainment velocities across the density interface. By choosing the virtual origin exactly at the mid-position of the grid, his results clearly showed that the power, ranging from -0.8 to -1.5, was dependent on the stroke and the distance away from the grid. Nokes' study thus implied that the decay of the turbulent velocity might not be represented by the simple power law with n = 1. However, it should be noted that a value of n other than one leads to an invalidation of the dimensional homogeneity in (1).

In this study, we employ the Digital Particle Image Velocimetry (DPIV) technique to investigate the turbulence induced by an oscillating-grid. The two main advantages of this technique over the other approaches are (a) it is non-intrusive and (b) the planar measurements that are taken simultaneously allow a direct evaluation of the spatial correlation of the velocity fluctuations. The spatial decay of the turbulence generated and its horizontal homogeneity are re-examined in details using the new experimental data.

EXPERIMENTAL APPARATUS AND PROCEDURES

Oscillating Grid System

Fig. 1(a) shows a schematic representation of the turbulence-generating system used in this study, which was very similar to those used by other researchers (see Table 1). The water tank was made of glass and had a dimension of 50cm×50cm in cross section and 100cm in height. Its transparent walls and bottom allowed the projection of laser sheets as well as the subsequent image capturing. The tank was supported by a platform, of which the height was adjustable. A grid made of square bars of 1cm×1cm had a mesh size of 5cm, giving a solidity of 36%. A solidity lower than 40% was considered to be capable of effectively avoiding strong inhomogeneity and secondary circulation (De Silva and Fernando, 1992). The grid was hanged vertically at the middle of the water depth of 60cm by four steel bars with 0.5cm diameter, which were connected to a speed-controlled motor.

To obtain a homogenous turbulence field, the grid arrangement was further improved by designing its end condition in such a way that the wall acted as a plane of symmetry. This type of setup was found to be able to effectively avoid unexpected secondary flows. Another grid that did not have this wall condition was also tested in this study and the results showed that the secondary flow was obviously stronger. This wall condition is consistent with the suggestion given by E and Hopfinger (1986), who stated that the turbulence is strongly affected by the grid geometry near the wall. In addition, the gap between the glass wall and the ends of the grid bars was set as small as 0.2~0.3cm to further avoid undesirable influence of the end condition. The grid system was oscillated vertically with a stroke of 4cm at 1 to 4 Hz. Since the oscillating grid turbulence is sensitive to the initial conditions, data acquisition would only be initiated after at least twenty minutes from the start of the oscillation.

Digital Particle Image Velocimetry (DPIV)

The horizontal and vertical velocities were measured using the Digital Particle Image Velocimetry (DPIV) technique, which can be conveniently employed to obtain the planar flow distribution in an area to be sampled (Willert and Gharib, 1991). This is an important advantage compared to point-based velocimetry techniques like LDA and ADV. The DPIV technique has emerged as the digital counterpart of the conventional Laser Speckle Velocimetry and the film-based Particle Image Velocimetry (PIV) techniques. It enables two-dimensional digital images to be captured, viewed and processed at real time. Therefore, real-time modifications of the seeding density, illumination and other experimental parameters can be performed. In this study, a Dantec DPIV system was used that includes a dual-cavity frequency-induced Q-switched pulsed mini Nd:YAG laser with an energy level of 25 mJ per pulse, a Kodak Megaplus ES1.0 CCD camera with a resolution of 1008x1018 pixels, and the PIV 2000 Processor. This system has been successfully implemented in combination with Planar Laser Induced Fluorescence (PLIF) by Law and Wang (2000) to study the mixing processes induced by buoyant jets. Its performance was verified with good agreement between the experimental results obtained and the existing point-based measurements.

The typical processes involved in DPIV data acquisition consist of seeding, illumination, recording and data analysis. Polyamid particles with a nominal diameter of 50 μm were used as flow field tracers. Seeding density was adjusted to ensure that about 8~10 particles were usually observed within an interrogation area. The two laser beams from the dual pulsed laser were aligned such that the two vertical light sheets illuminated the same spatial area. The pulse duration and the pulse interval were much smaller than the time scale of the flow so that the measured velocities can be considered to be instantaneous values. The pulse duration was about 7 ns, while the pulse interval ranged from 8 to 65ms and was optimised for each test to achieve a maximum displacement of about 8 pixels, i.e., 25% of the side of the interrogation area. The light sheet had a typical thickness of 0.3cm and a divergence angle of 32^o.

Images with a size of approximately 10cm×10cm were taken at a few locations in the flow field, of which a plan view is provided in Fig. 1(b). The camera, with its axis perpendicular to the laser sheet, was adjusted with slight defocusing such that the size of a seeding particle was generally greater than 3 pixels. This size was necessary to enhance the accuracy of the sub-pixel interpolation. The camera was equipped with a CCD chip of 0.91×0.92cm, having an intensity resolution of 8 bits. The sampling rate was set at 5 Hz, which was directly limited by the maximum readout frequency for the double images being approximately 7 Hz. Cross-correlation analysis was performed to derive the velocity vectors from the images. The interrogation area was selected as 32×32 pixels with an overlap of 25%. The overlap does not increase the resolution of DPIV but does provide more spatial information for the cross-correlation calculations especially at the edge of the interrogation area.

The sampling duration was set to be 100s, i.e., 500 images were taken at each location. This duration was determined based on the results of the calibration tests, which were conducted to explore the effect of the number of image pairs on the statistical results of the velocity fluctuations. An example of the horizontal velocity fluctuations, which were obtained in the calibration tests at three different elevations at Section B, is presented in Fig. 2, where the number of image pairs used in the averaging calculations ranges from 1 to 500. It clearly demonstrates that the statistical results are not consistent for small samples and only approach a constant when the number of image pairs exceeds approximately 400. This observation implies that low accuracy may be associated with the statistical results in Lyn (1997) that were obtained based on only 25 to 36 images.

RESULTS

As shown in Fig. 1(b), two typical sections parallel with each other, Sections B and H, located within one quarter of the grid plane, were selected for the measurements. Section B was aligned with the bar location, while Section H was located through the grid openings. It was anticipated that the two sections would have different turbulence characteristics because vortices were directly shed from the bar when the grid was oscillated. Each section was composed of four imaging areas with 50% overlap in the horizontal direction, of which the two lower areas were chosen just above the top position of the oscillating grid and the upper areas were set approximately 4 cm below the water surface. Verification tests with different water depths were performed to confirm that the water surface effect on the velocity fluctuations is insignificant in the imaged areas selected. As shown in Fig. 1, the vertical coordinate z was set upward originating from the mid-plane of the grid and the horizontal coordinate x was directed from the centreline of the mid-plane to the glass wall of the tank.

As stated previously, 500 image pairs with an area of 10cm×10cm were taken within 100s for each location. For each image, 41×42 velocity vectors were then derived using the cross-correlation approach. This allows the computation of temporally averaged characteristics of the turbulence for each point in the imaged area as well as their spatial variations. Subsequently, the characteristics were spatially averaged at each elevation for further analysis. In the following, the temporally averaged characteristics of the turbulence are first reported. The spatially averaged velocity fluctuations are then presented in comparison with the previous results.

Fig. 3 shows the distributions of the temporally averaged values of the velocity fluctuations and Reynolds shear stresses at different elevations at Sections B and H, respectively. The results plotted are taken, as an example, from the imaged areas close to the centre of the water tank with the grid oscillating at 4 Hz. Similar results can be obtained with other oscillating frequencies from 1 to 3 Hz. In Figs 3(a) and 3(b), significant horizontal variations of the measured velocity fluctuations can be observed at a small distance from the grid, say, at z = 5 cm. These variations near the grid are even more prominent for the vertical velocity fluctuations. With increasing distance from the grid, the turbulence becomes more homogeneous in the horizontal plane and the variations in the velocity fluctuations reduce. Furthermore, it can be seen in Figs. 3(a) and 3(b) that the velocity fluctuations for Section B are enhanced at the locations immediately above the bar intersections, i.e., x = 2~3 cm and 7~8 cm. This is probably due to the interactions of the vortices shed from the bars, which are aligned in the two directions perpendicular to each other.

Correspondingly, as shown in Fig. 3(c), the distribution of the Reynolds shear stresses clearly indicates that the turbulence can be considered to be shear-free only at a distance sufficiently far away from the grid, where the Reynolds shear stress approaches zero. In comparison, the Reynolds shear stress obviously deviates from zero, especially at Section B, in the region near the grid.

The various distributions of turbulence characteristics at different elevations shown in Fig. 3 demonstrate that the mechanism of turbulence generation is comparable with the qualitative observations reported in Hopfinger and Toly (1976) and Nokes (1988). Generally two kind of flows, namely jets and wakes, can be identified with the grid oscillation. The jets are formed throughout the grid openings and the wakes are created below and above the bars. Whether the jets or wakes are dominant depends on the grid geometry. For a grid with a high solidity like a plate with small holes, jets are important in generating the turbulence away from the grid. In comparison, for a grid with a low solidity like the 36% used in this study, the turbulence is formed primarily by the interaction of the wakes. This is why the near-grid turbulence shows higher intensity shear at Section B instead of Section H. The jets or wakes interact with each other, and the turbulence diffuses away from the grid. Shear-free turbulence with little or no mean horizontal variation finally occurs at a large enough distance from the grid.

To further describe the changes in the flow field from inhomogeneity to homogeneity, three vertical lines above the grid were selected as shown in Fig. 4. They are located at Position I at the bar intersection, Position H at the centre of the opening, and Position B in the middle of the two neighbouring intersections, respectively. Fig. 4(a) shows no clear differences of the horizontal velocity fluctuations among the three locations provided that the distance from the grid is greater than about 1.5 times the mesh sizes, i.e., 7.5cm. On the other hand, the distance needs to be more than three times the mesh sizes, i.e., 15cm, to ensure a uniform distribution of the vertical velocity fluctuations at the three locations. In other words, homogeneous turbulence can be achieved only when the distance is more that three mesh sizes away from the grid mid-plane. Such a critical distance is consistent with the results obtained in the following section based on the spatially averaged turbulence velocity.

Spatially Averaged Velocity Fluctuations

To compare the present results with the empirical scaling law for the turbulence decay as shown in (1), the measurements of the velocity fluctuations were further averaged spatially at each elevation for Sections B and H. The results of the horizontal velocity fluctuation, presented in Fig. 5, show that the near-grid turbulence at Section B is stronger than that at Section H. The difference between the two sections becomes insignificant when the distance from the grid is greater than about three mesh sizes, i.e., z = 15cm. It is also interesting to note that (1) seems to represent an upper bound of the horizontal velocity fluctuations, which is close to the measurements taken at Section B.

The profiles given in Fig. 5 for Sections B and H were further averaged to represent the vertical variations of the turbulence characteristics. It is assumed that changes in the characteristic turbulent values from Section B to Section H are linear. The computed results are shown in Fig. 6, where (1) is also fitted to the data with slight changes in the coefficient C. The C-values for f = 2-4 Hz are all close to 0.25 given by Hopfinger and Toly (1976) except for a smaller value used for the case of f = 1 Hz.

Integral Length Scale and its Implication in Turbulence Decay

An important advantage of the DPIV technique pertaining to the current analysis is that the planar velocity measurements were taken simultaneously, enabling a direct evaluation of the spatial correlation of velocity fluctuations over the imaged area. The integral length scale can thus be computed using the longitudinal and transverse correlation coefficients, respectively, as follows:

$$\Lambda_f = \int_o^\infty f(\zeta)d\zeta \tag{2}$$

$$\Lambda_g = \int_o^\infty g(\zeta)d\zeta \tag{3}$$

where f(ζ) = longitudinal correlation coefficients and g(ζ) = transverse correlation coefficients. As an example, Fig. 7 shows the correlation coefficients computed for f = 4Hz at Section B. In the computations, the longitudinal and transverse correlation coefficients were first evaluated for each imaged area and then ensemble averaging was performed using all the 500 vector maps for the case studied. Fig. 7 clearly shows that the correlation coefficients for small distance lags increase with increasing distance from the grid. The computed integral length scale is plotted in Fig. 8 against z. The length scale is normalised with z to examine whether the ratio of the length scale to the distance, β, is constant, as suggested in the previous studies. The results show that the ratio is indeed almost constant independent of the distance, although it appears to be slightly larger in the region near the grid than far away from the grid. In other words, the length scale is almost proportional to the distance from the grid. The coefficients of proportionality, which are derived from the longitudinal correlation coefficient, range from 0.1 to 0.2, while those derived from the transverse correlation coefficient vary from 0.06 to 0.17. The proportionality factor for the longitudinal correlation coefficient is larger than the value given by Hopfinger and Toly (1976), who reported that the longitudinal length scale computed from the auto-covariance of the velocity signal is approximately 0.1 times the distance from the virtual origin of the grid. As noted in previous studies, large-scale circulations driven by the oscillating grid turbulence may cause uncertainty in the integral length scale. These circulations could not be avoided completely despite the careful experimental set-up. However, it is found here that this problem can be effectively overcome through spatial- and ensemble-averaging computations. Similar conclusion was also drawn by Brumley and Jirka (1987) in the analysis of their data collected using a rotating hot-film probe.

With the assumption of the length scale being proportional to z, the eddy viscosity, ν_t, can thus be expressed in the form (Rodi, 1993)

$$\nu_t = c'_\mu \beta \sqrt{k} z \tag{4}$$

where c_μ' = empirical constant. On the other hand, the k-equation reads

$$\frac{\partial}{\partial z}\left(\frac{\nu_t}{\sigma_k}\frac{\partial k}{\partial z}\right) = c_D \frac{k^{\frac{3}{2}}}{\beta z} \tag{5}$$

where σ_k, c_D = constants. Substituting (4) into (5) and then solving yields

$$k^{\frac{3}{2}} = c_1 z^{\sqrt{c}} + c_2 z^{-\sqrt{c}} \tag{6}$$

where c_1, c_2 = constants and $c = (1.5 c_D \sigma_k) / (c'_\mu \beta^2)$. Since k should approach zero with large distance, c_1 should thus be equal to zero and (6) changes to

$$k = c_2^{\frac{2}{3}} z^{-\frac{2\sqrt{c}}{3}} \tag{7}$$

Eq. (7) shows that the turbulence kinetic energy and thus the velocity fluctuation decays with increasing distance in the manner of the power law, which is consistent with (1). The above derivation suggests that the power-law decay of grid turbulence is closely related to the fact that the length scale is proportional to the distance from the grid plane. It should be noted that by analogy with the temporal change of energy in homogeneous turbulence, Thompson and Turner (1975) previously provided a slightly different derivation that also yields the power-law decay of the turbulence velocity.

CONCLUSIONS

DPIV technique was employed to study the distribution of turbulence generated in a water tank by a vertically oscillating grid. The experimental results basically confirm the previous findings obtained based on accurate point-based measurement techniques. Furthermore, the present study quantitatively reveals the flow structure in the region near the grid. It was found that the structure is closely related to the grid geometry. The intensity of the near-grid turbulence is clearly enhanced in the region near the bar intersections. Shear flow exists near the grid and the turbulence generated can be considered to be horizontally homogeneous only when the distance from the grid mid-plane is more than approximately three mesh sizes. This study also shows that the turbulence decay follows the power law if the length scale increases linearly with the distance from the grid plane. The information presented in this paper should be helpful for the planning of future studies related to applications of the oscillating grid turbulence.

APPENDIX I. REFERENCES

1. Brumley, B. H. and Jirka, G. H. (1987). "Near-surface turbulence in a grid-stirred tank." J. Fluid Mech., 183, 235-263.

2. Brunk, B., Weber-Shirk, M., Jensen, A., Jirka, G., and Lion, L. W. (1996). "Modeling natural hydrodynamic systems with a differential-turbulence column." J. Hydr. Engrg., ASCE, 122(7), 373-380.
3. De Silva, I. P. D., and Fernando, H. J. S. (1992). "Some aspects of mixing in a stratified turbulent patch." J. Fluid Mech., 240, 601-625.
4. E, X. and Hopfinger, E. J. (1986). "On mixing across an interface in stably stratified fluid." J. Fluid Mech., 166, 227-244.
5. Ettema, R., Karim, F. and Kennedy, J. F. (1984). "Laboratory experiments on frazil ice growth in supercooled water." Cold Regions Science and Technology, 10(1), 43-58.
6. Hopfinger, E.J. and Toly, J.A. (1976) "Spatially decaying turbulence and its relation to Mixing across density interfaces." J. Fluid Mech., 87, part 1, 155-175.
7. Jirka, G. H. (1991). "Gas transfer processes at the air/water interface." Environmental Hydraulics, J. H. W. Lee, and Y. K. Cheung, eds. Balkema, Rotterdam, The Netherlands. 357-370.
8. Law, A.W.K. and Wang, H.W. (2000). "Measurements of mixing processes with Combined Digital Particle Image Velocimetry and Planar Laser Induced Fluorescence." Experimental Thermal and Fluid Science. (In press).
9. Lyn, D. A. (1995). "Observations of initial sediment motion in a turbulent flow generated in a square tank by a vertically oscillating grid." Proc. 1st International Conference on Water Resources. ASCE, New York. Vol.1, 608-612.
10. Lyn, D. A. (1997). "A PIV study of an oscillating-grid flow." Experimental and Numerical Flow Visualization and Laser Anemometry, American Society of Mechanical Engineers, Fluids Engineering Division (Publication). ASME, New York. Vol. 13, 6p.
11. McDougal, T. J. (1979). "Measurements of turbulence in a zero-mean-shear mixed layer." J. Fluid Mech., 94, 409-431.
12. Nielsen, P. (1993). "Turbulence effects on the settling of suspended particles." J. Sedimentary Petrology, 63(5), 835-838.
13. Nokes, R. I. (1988). "On the entrainment rate across a density interface." J. Fluid Mech., 188, 185-204.

14. Rodi, W. (1993). Turbulence Models and Their Application in Hydraulics: A State-of- the-Art Review. A. A. Balkema, The Netherlands.
15. Rouse, H. (1939). "Experiments on the mechanics of sediment suspension." Proc. 5th International Congress of Applied Mechanics, Cambridge, MA, 550-554.
16. Thompson, S. M., and Turner, J. S. (1975). "Mixing across an interface due to turbulence generated by an oscillating grid." J. Fluid Mech., 67, 349-368.
17. Willert, C. E. and Gharib, M. (1991). "Digital particle image velocimetry." Experiments in Fluids, 10, 181-193.

APPENDIX II. NOTATION

The following symbols are used in this paper:

C = constant;

c = constant;

c_D = constant;

c_1, c_2 = constants

c_μ' = constant;

f = frequency of oscillation;

$f(\zeta)$ = longitudinal correlation coefficient;

$g(\zeta)$ = transverse correlation coefficient;

k = turbulent kinetic energy;

M = mesh size;

N = averaging window size;

n = power;

S = stroke;

u = r.m.s. value of horizontal velocity fluctuation;

$-\overline{uv}$ = Reynolds shear stress;

v = r.m.s. value of vertical velocity fluctuation;

x = horizontal distance from the centreline of the grid;

z = vertical distance from the grid mid-plane;

z_v = vertical distance from the virtual origin;

Λ_f = longitudinal integral length scale;

Λ_g = transverse integral length scale;

β = ratio of the length scale to the distance from the grid;

ν = kinematic viscosity of fluid;

ν_t = eddy viscosity;

σ_k = constant; and

ζ = distance lag.

Captions for Figures

Fig. 1.	**Sketch of Experimental Setup. (a) Water Tank; (b) Plan View of Imaged Locations.**
Fig. 2.	**Variations of Horizontal Turbulence Intensity with Number of Vector Maps for Averaging Calculations.**
Fig. 3(a).	**Distributions of Horizontal Velocity Fluctuations at Sections B and H.**
Fig. 3(b).	**Distributions of Vertical Velocity Fluctuations at Sections B and H.**
Fig. 3(c).	**Distributions of Reynolds Shear Stresses at Sections B and H.**
Fig. 4(a).	**Vertical Profiles of Relative Horizontal Velocity Fluctuation at Different Positions.**
Fig. 4(b).	**Vertical Profiles of Relative Vertical Velocity Fluctuation at Different Positions.**
Fig. 5.	**Decay of Spatially Averaged Horizontal Velocity Fluctuation at Sections B and H in Comparison with Eq. (1).**
Fig. 6.	**Turbulence Decay Following the Power-Law Formula.**
Fig. 7.	**Longitudinal and Transverse Correlation Coefficients at Different Elevations.**
Fig. 8.	**Variations of Ratio of Integral Length Scales to Distance From Grid.**

Table 1. Experimental Conditions for Turbulence Generation by an Oscillating Grid

Researchers	Tank dimensions			Grid description		Oscillating frequency f (Hz)	Stroke S(cm)	Measurement technique
	Length (cm)	Width (cm)	Height (cm)	Mesh size M(cm)	Bar section (cm x cm)			
Thompson and Turner (1975)	25.4	25.4	46	5	1×1	2-5	1	Hot-film
Hopfinger and Toly (1976)	67.5	67.5	100	5,10	1×1,2×2	2-6	4,9	Hot-film
McDougal (1979)	25.4	25.4	46	5	1×1	1-10	1	LDA
Brumley and Jirka (1987)	50	50	40	6.35	1.3×1.3	1.15-3.79	2.16-9.9	Hot-film
Nokes (1988)	25.4	25.4	60	5	1×1	4	0.77-4.9	-
De Silva and Fernando (1992)	26	26	60	2.93,4.76,6.2	0.9×0.9	1-5	0.85,2.1	LDV
Lyn (1997)	25.4	25.4	48	4.8	0.95×0.95	4.6	5.08	PIV
Present study	50	50	100	5	1×1	1-4	4	DPIV

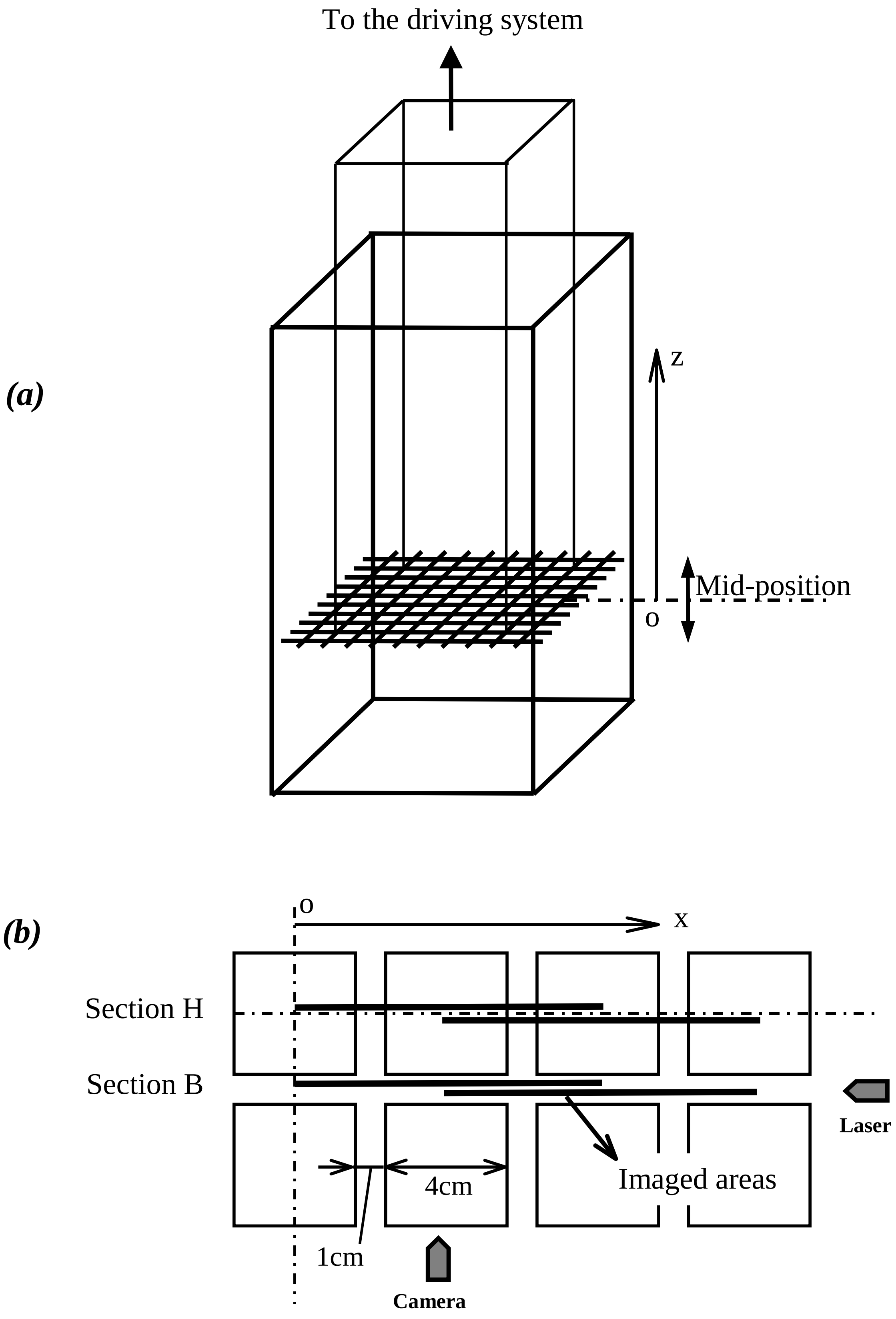
To the driving system
(a)
z
Mid-position
o
(b)
o
x
Section H
Section B
Laser
4cm
Imaged areas
1cm
Camera

Fig 1

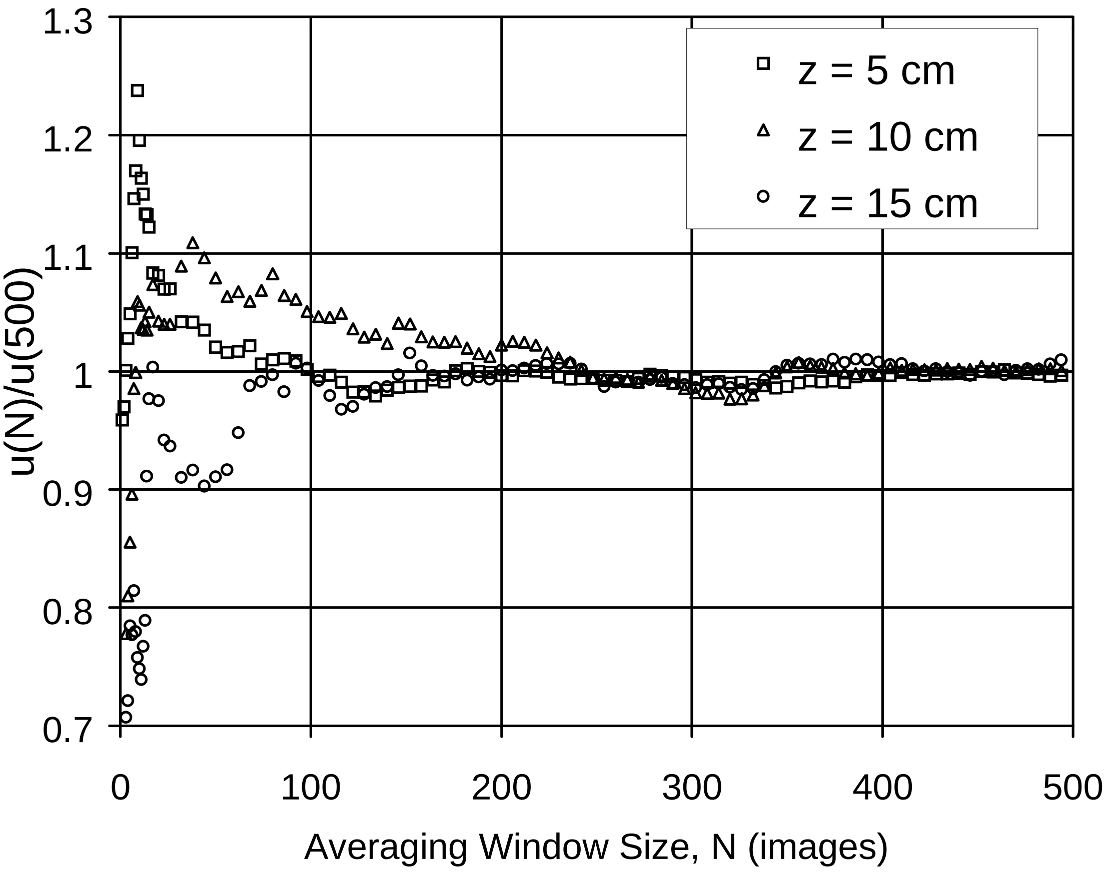
1.3
1.2
1.1
1
0.9
0.8
0.7
u(N)/u(500)
0
100
200
300
400
500
Averaging Window Size, N (images)
z = 5 cm
z = 10 cm
z = 15 cm

Fig 2

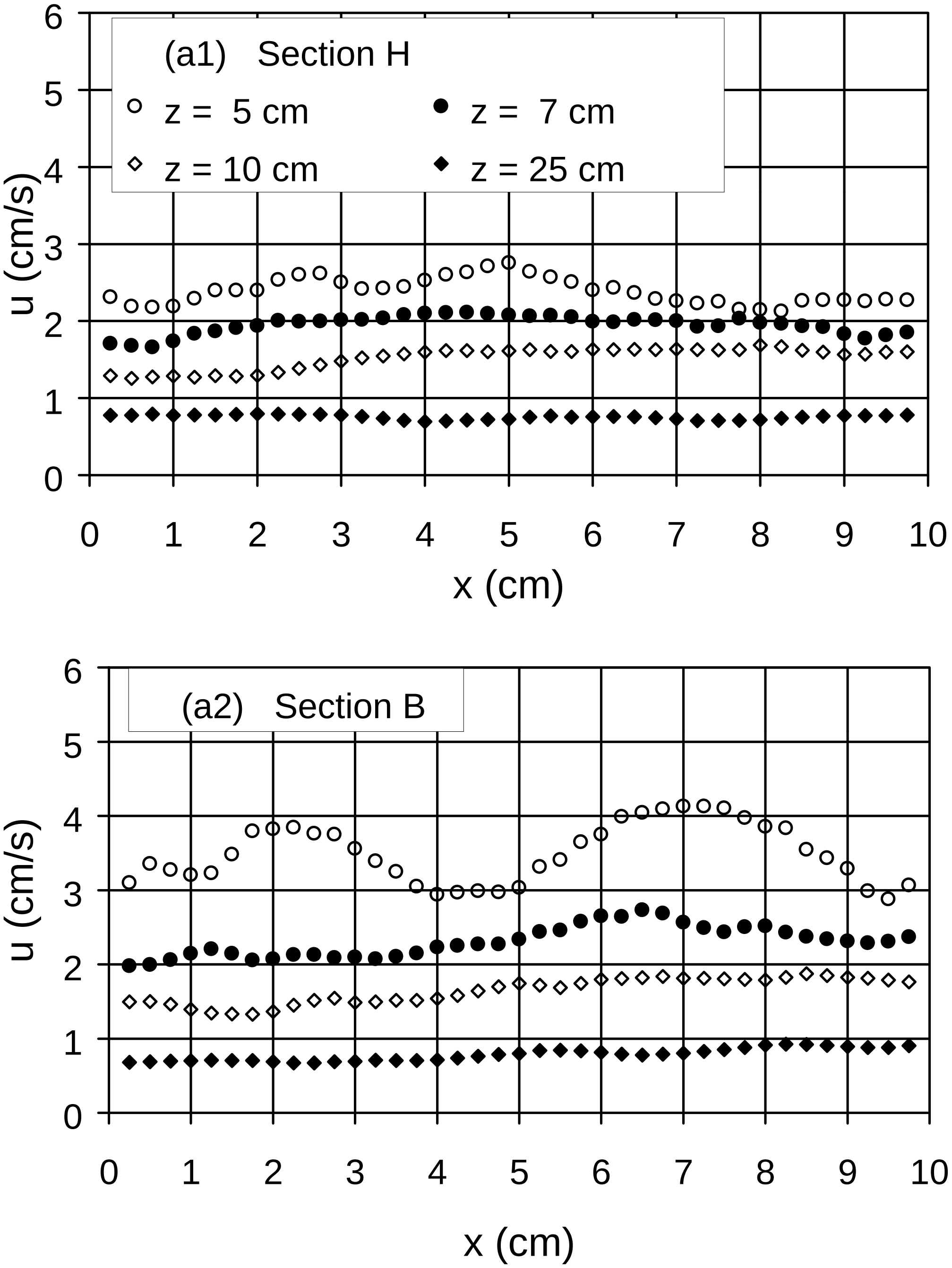
(a1) Section H
○ z = 5 cm
● z = 7 cm
◇ z = 10 cm
◆ z = 25 cm
u (cm/s)
0
1
2
3
4
5
6
x (cm)
0
1
2
3
4
5
6
7
8
9
10
(a2) Section B
u (cm/s)
0
1
2
3
4
5
6
x (cm)
0
1
2
3
4
5
6
7
8
9
10

Fig 3(a)

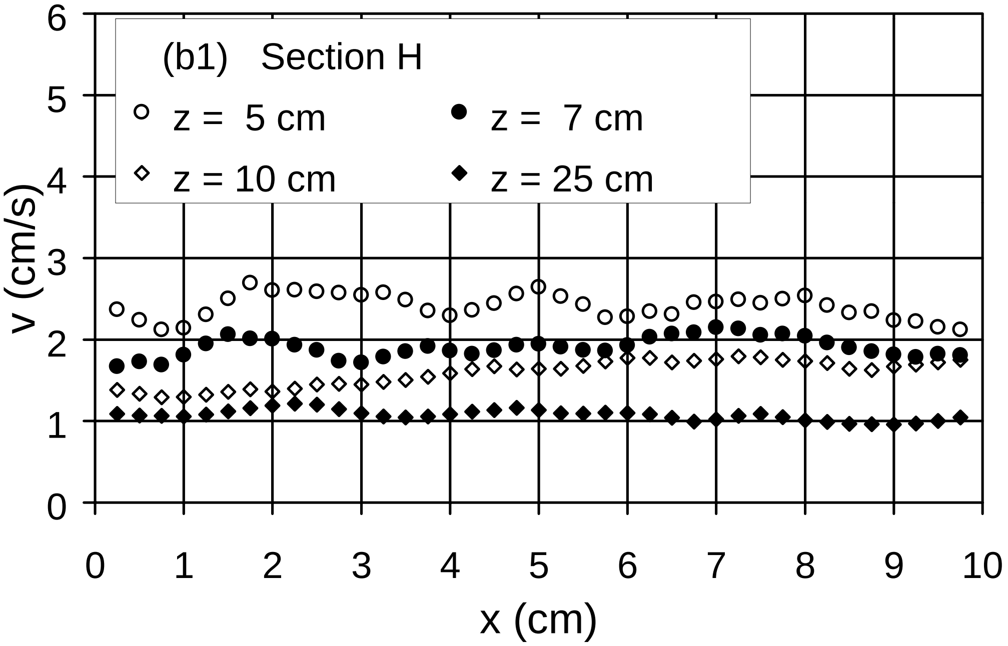
(b1) Section H
○ z = 5 cm
● z = 7 cm
◇ z = 10 cm
◆ z = 25 cm
v (cm/s)
0
1
2
3
4
5
6
x (cm)
0
1
2
3
4
5
6
7
8
9
10

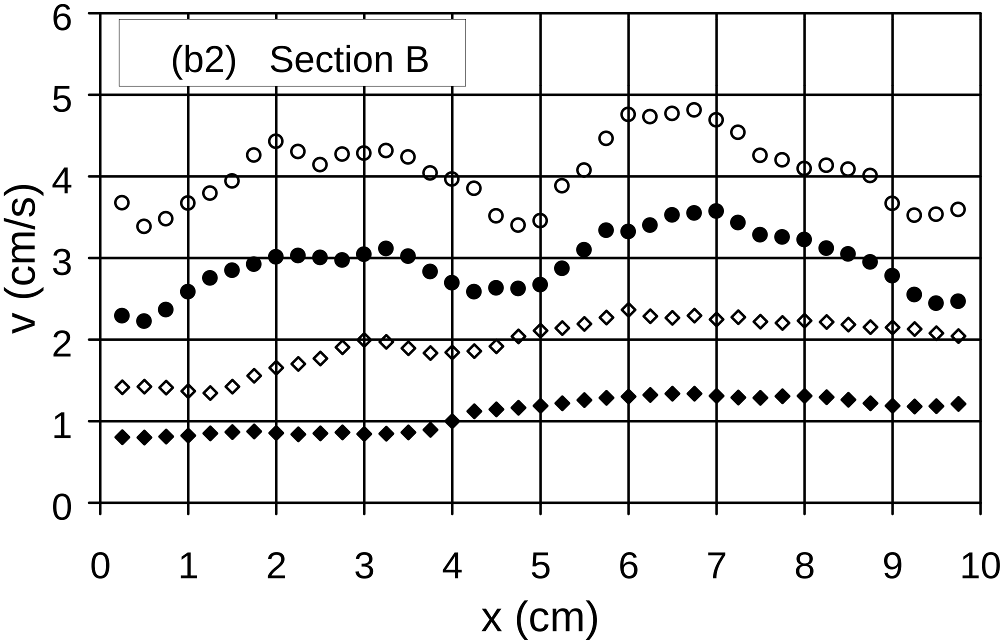
(b2) Section B
v (cm/s)
0
1
2
3
4
5
6
x (cm)
0
1
2
3
4
5
6
7
8
9
10

Fig 3(b)

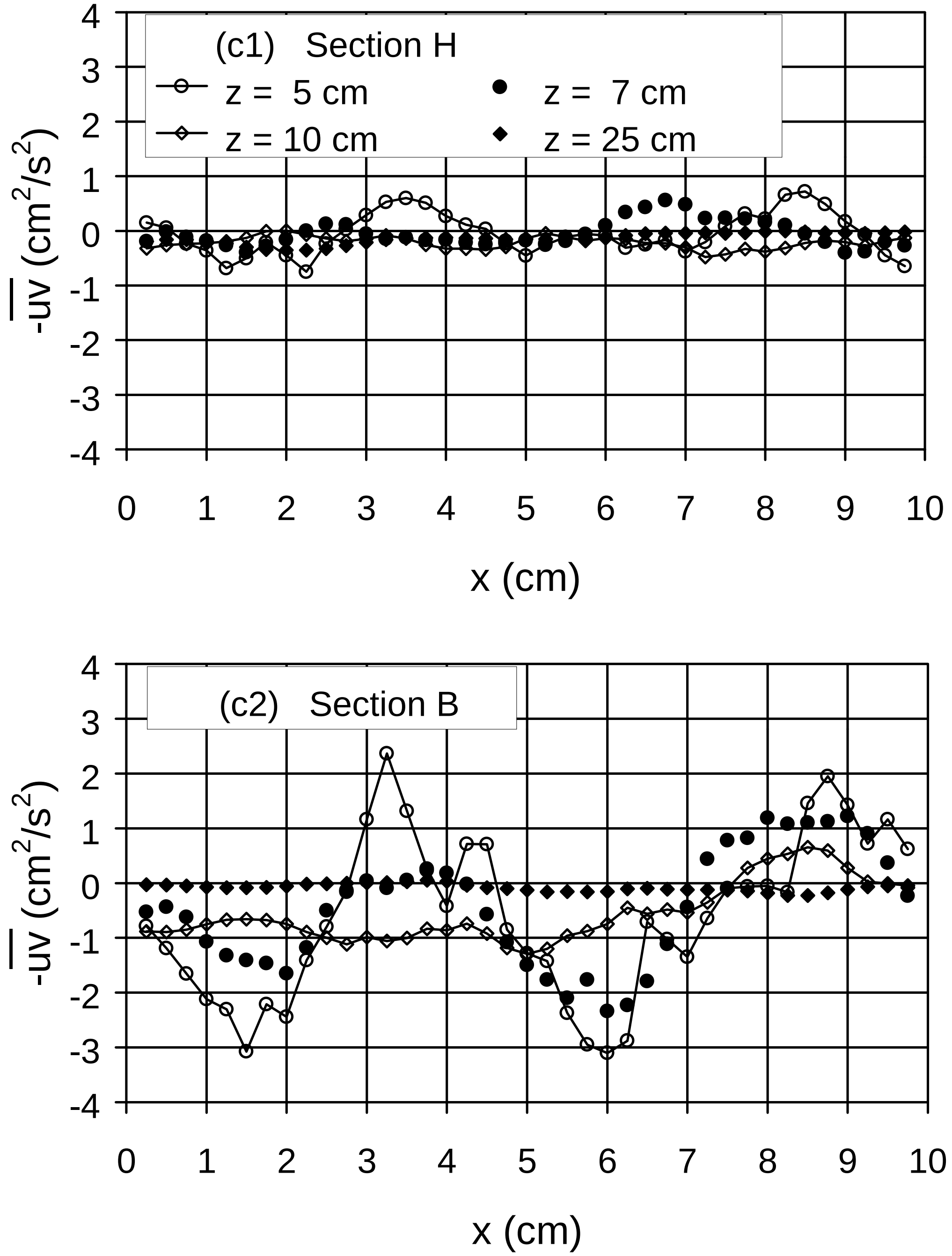
(c1) Section H
z = 5 cm
z = 7 cm
z = 10 cm
z = 25 cm
$-\overline{uv}$ (cm^2/s^2)
4
3
2
1
0
-1
-2
-3
-4
0
1
2
3
4
5
6
7
8
9
10
x (cm)
(c2) Section B
$-\overline{uv}$ (cm^2/s^2)
x (cm)

Fig 3(c)

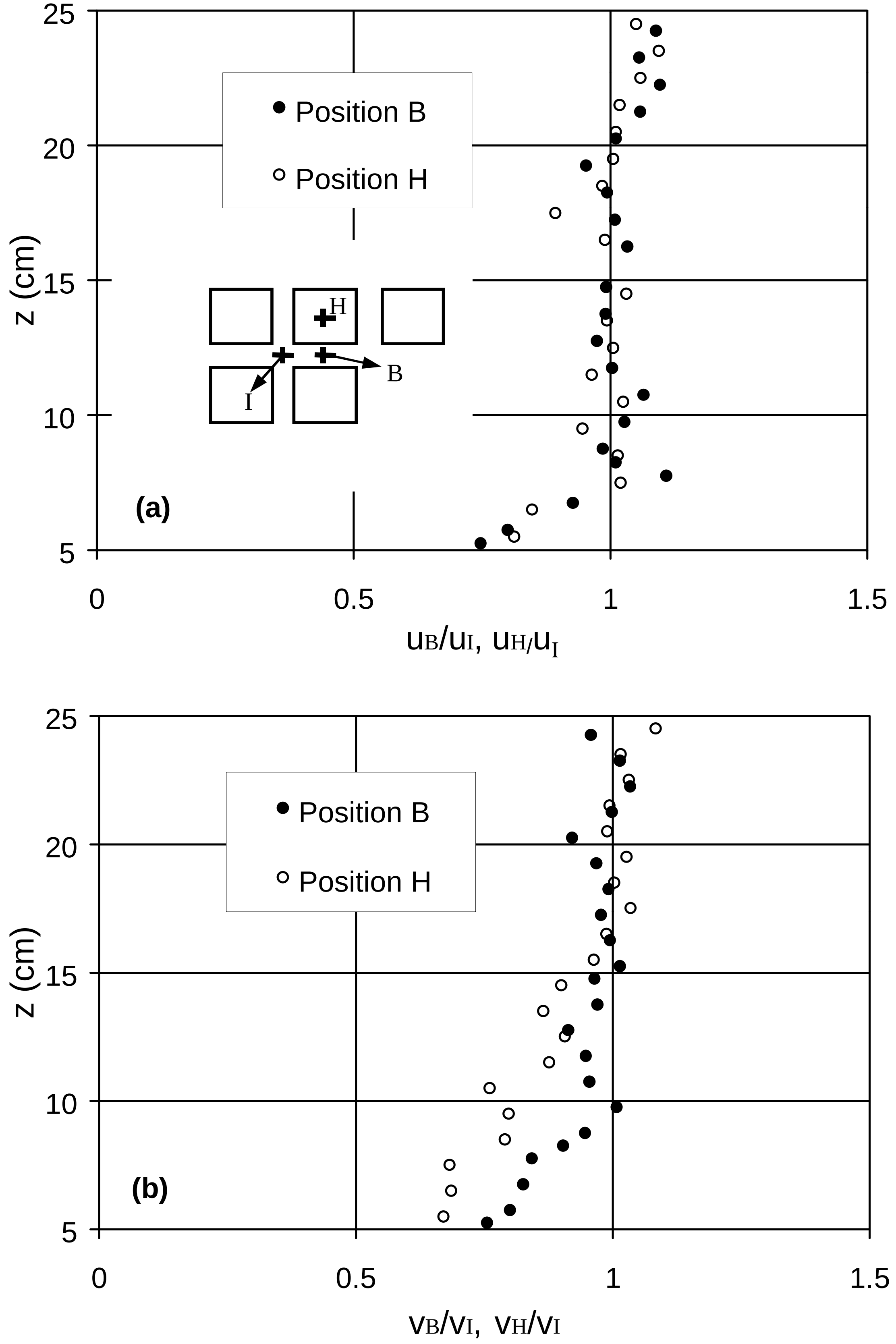
25
20
15
10
5
z (cm)
0
0.5
1
1.5
● Position B
○ Position H
H
B
I
(a)
uB/uI, uH/uI
25
20
15
10
5
z (cm)
0
0.5
1
1.5
● Position B
○ Position H
(b)
vB/vI, vH/vI

Fig 4(a)(b)

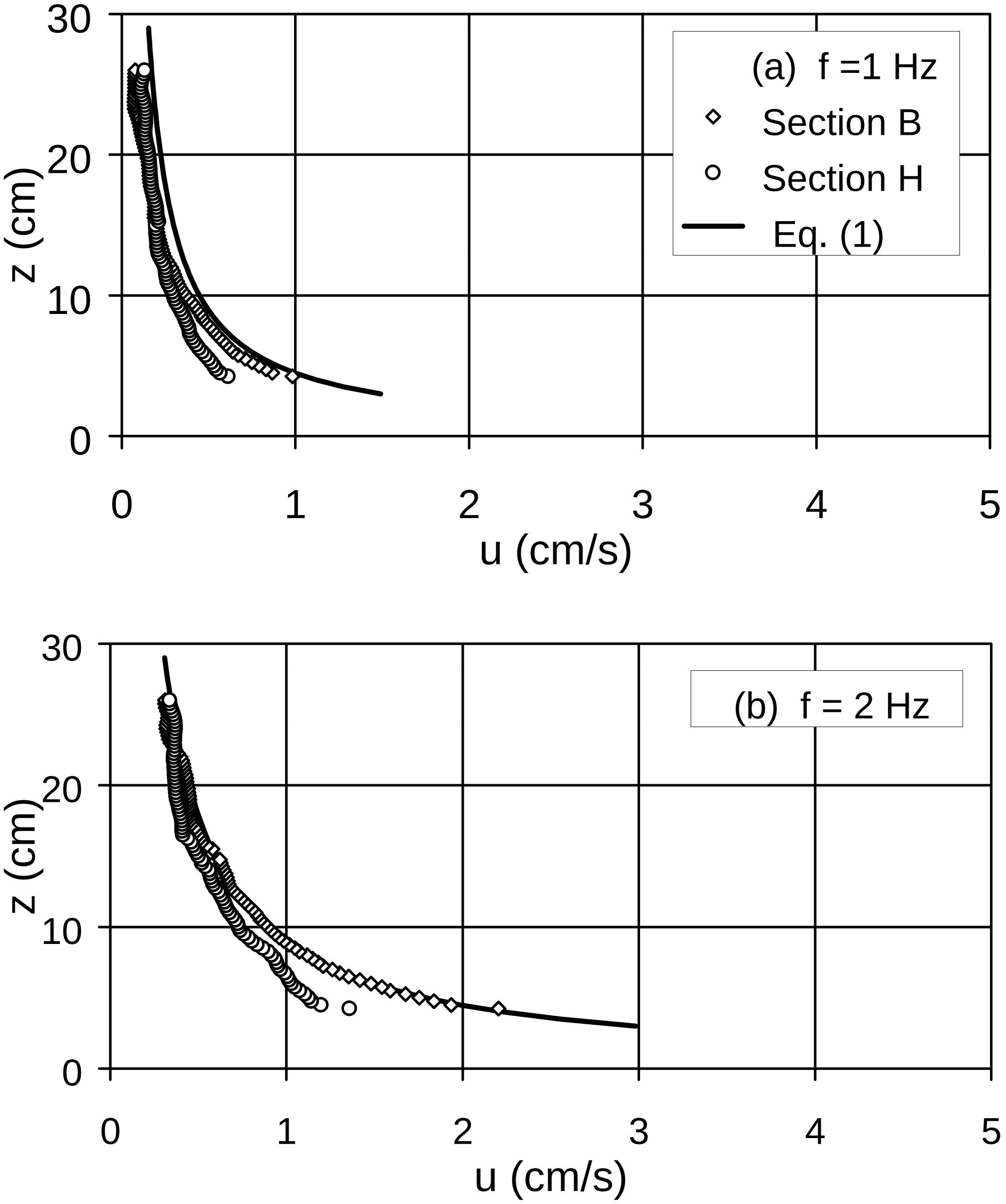
30
20
10
0
z (cm)
0
1
2
3
4
5
u (cm/s)
(a) f =1 Hz
Section B
Section H
Eq. (1)
30
20
10
0
z (cm)
0
1
2
3
4
5
u (cm/s)
(b) f = 2 Hz

Fig 5(a)(b)

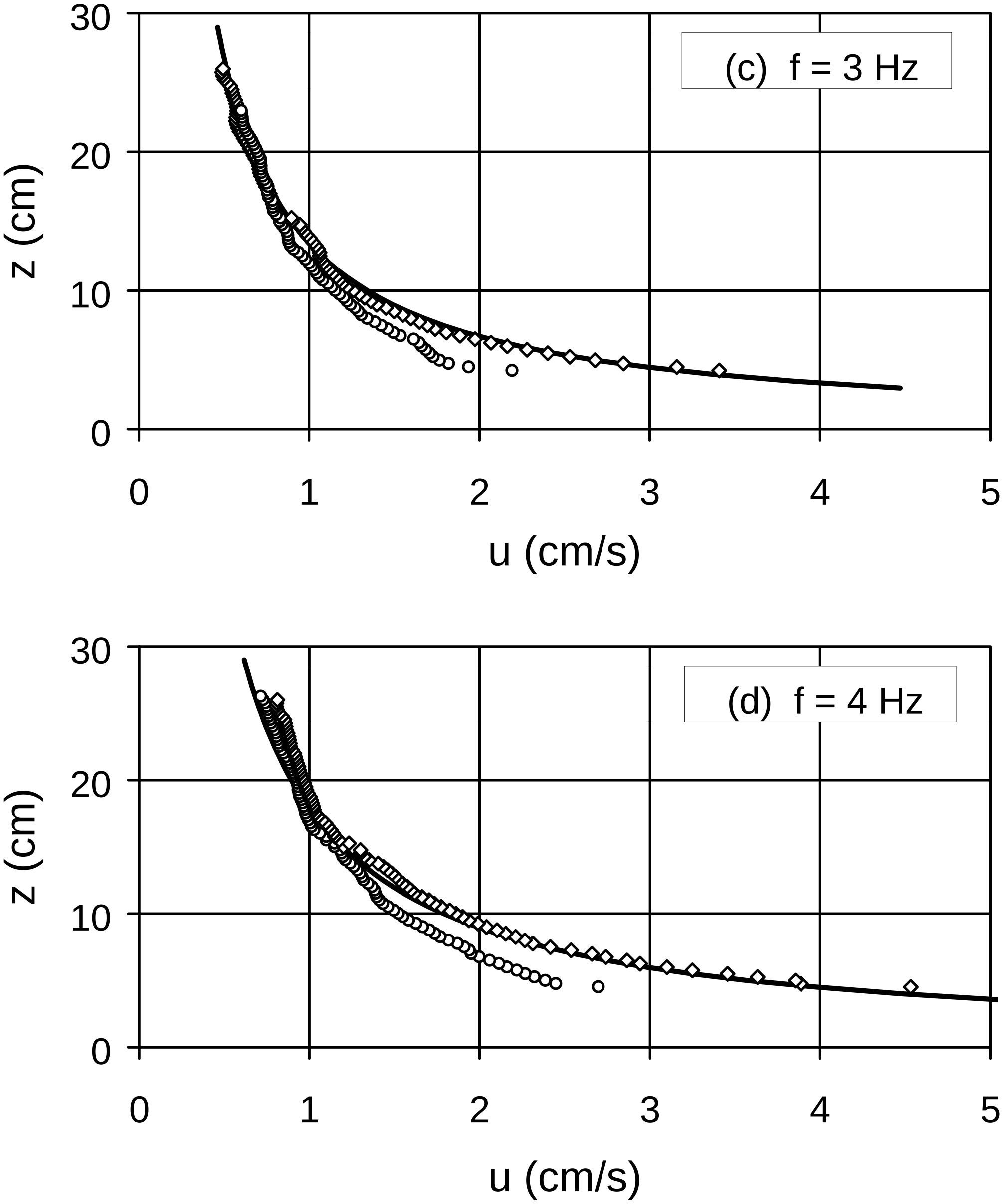
(c) f = 3 Hz
z (cm)
u (cm/s)
0
10
20
30
0
1
2
3
4
5
(d) f = 4 Hz
z (cm)
u (cm/s)
0
10
20
30
0
1
2
3
4
5

Fig 5(c)(d)

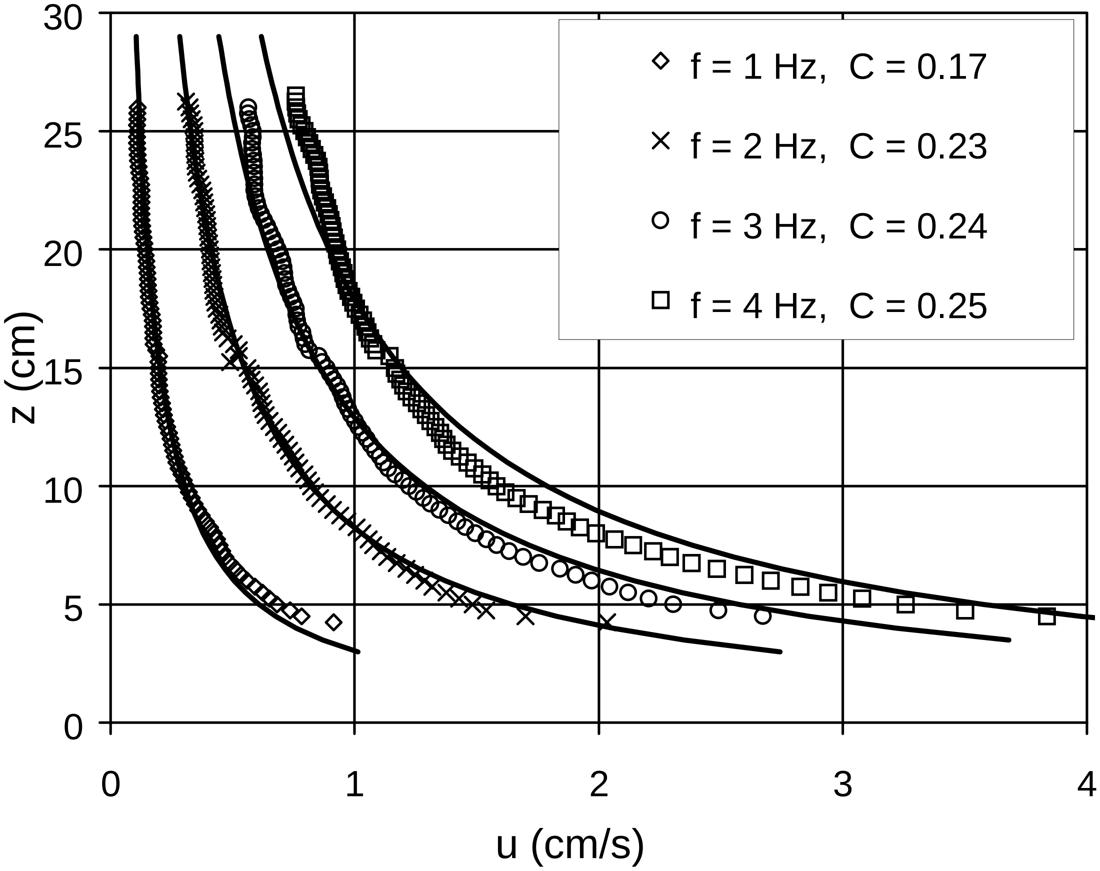
30
25
20
15
10
5
0
0
1
2
3
4
z (cm)
u (cm/s)
◇ f = 1 Hz, C = 0.17
× f = 2 Hz, C = 0.23
○ f = 3 Hz, C = 0.24
□ f = 4 Hz, C = 0.25

Fig. 6

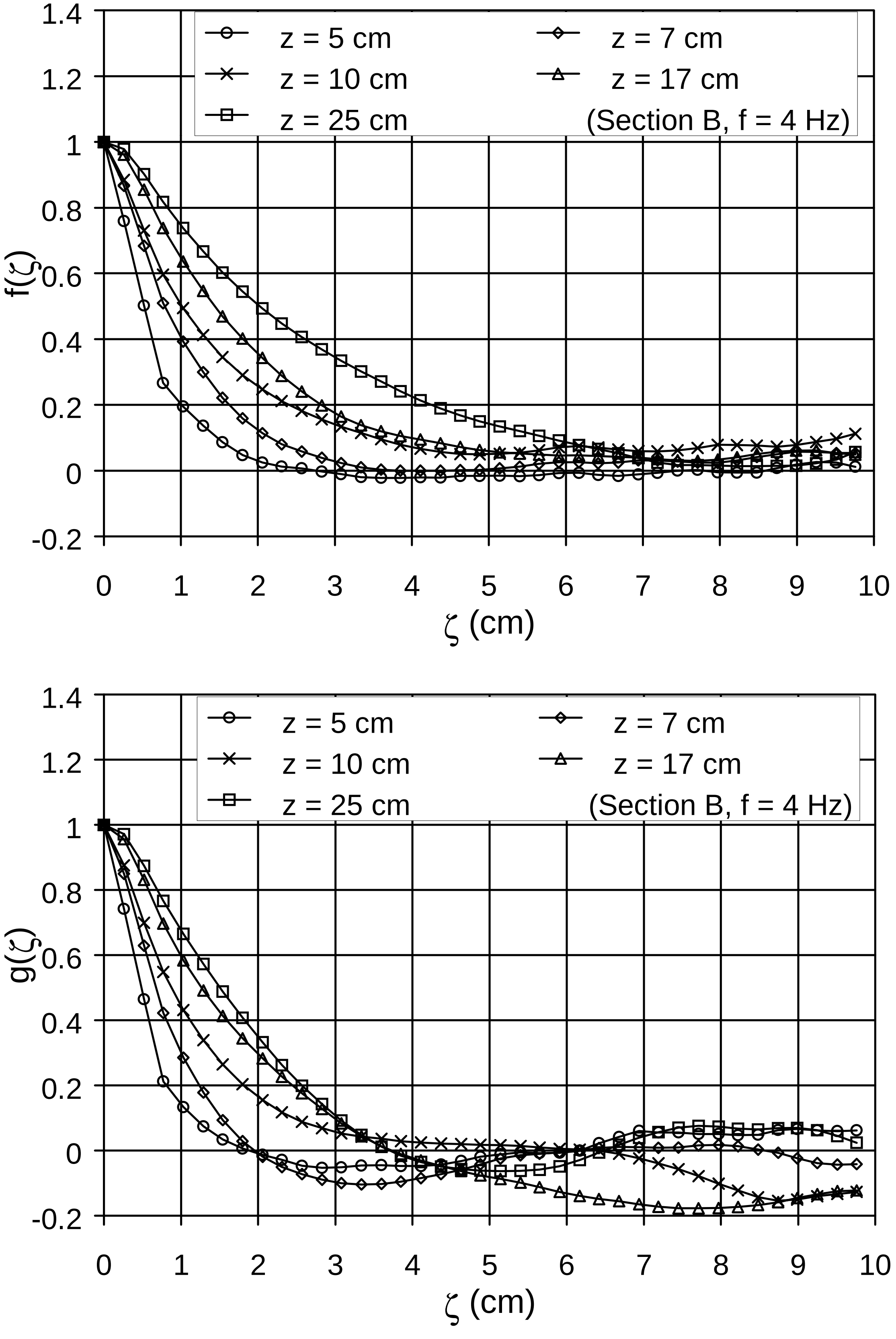
z = 5 cm
z = 7 cm
z = 10 cm
z = 17 cm
z = 25 cm
(Section B, f = 4 Hz)
f(ζ)
1.4
1.2
1
0.8
0.6
0.4
0.2
0
-0.2
0
1
2
3
4
5
6
7
8
9
10
ζ (cm)
z = 5 cm
z = 7 cm
z = 10 cm
z = 17 cm
z = 25 cm
(Section B, f = 4 Hz)
g(ζ)
1.4
1.2
1
0.8
0.6
0.4
0.2
0
-0.2
0
1
2
3
4
5
6
7
8
9
10
ζ (cm)

Fig. 7

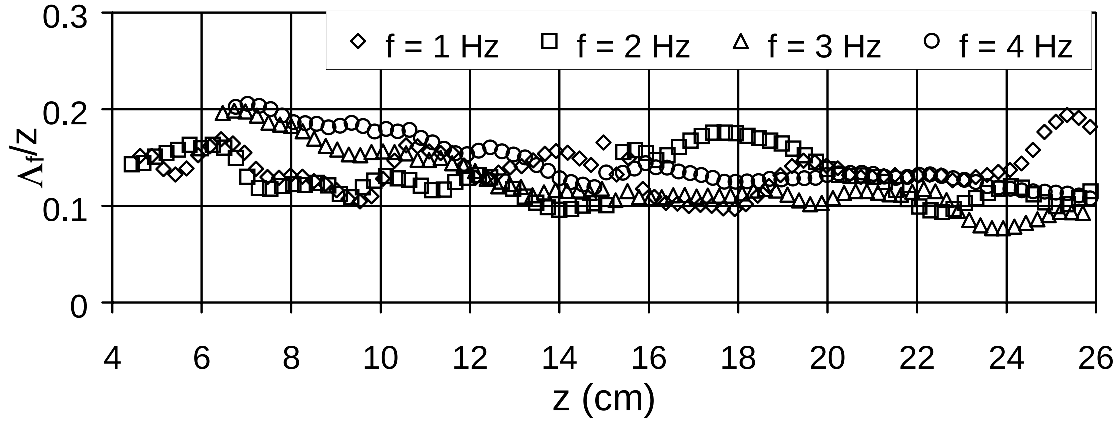
0.3
0.2
0.1
0
Λf/z
◇ f = 1 Hz
□ f = 2 Hz
△ f = 3 Hz
○ f = 4 Hz
4
6
8
10
12
14
16
18
20
22
24
26
z (cm)

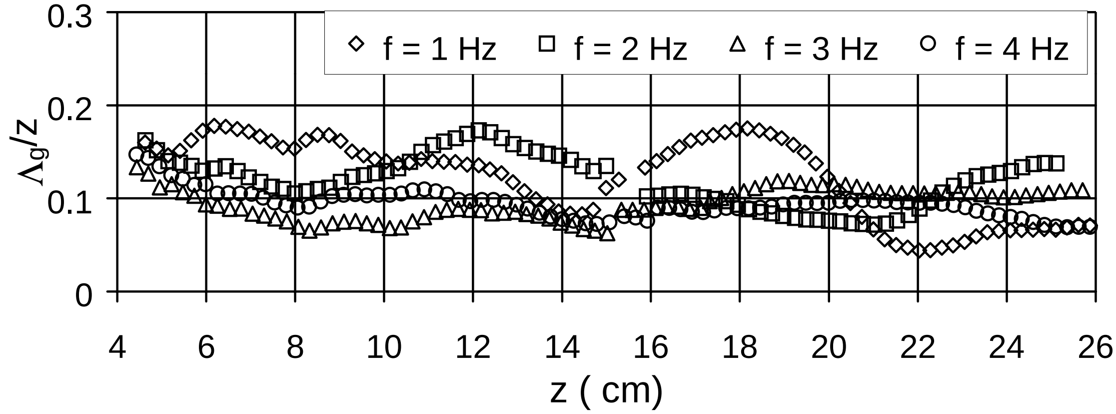
0.3
0.2
0.1
0
Λg/z
◇ f = 1 Hz
□ f = 2 Hz
△ f = 3 Hz
○ f = 4 Hz
4
6
8
10
12
14
16
18
20
22
24
26
z (cm)

Fig. 8